Tectonophysics 731–732 (2018) 172–180

Contents lists available at ScienceDirect

Tectonophysics

journal homepage: www.elsevier.com/locate/tecto

Constraints on fault and crustal strength of the Main Ethiopian Rift from formal inversion of earthquake focal mechanism data

Ameha A. Muluneh[a,*], Tesfaye Kidane[a,b], Giacomo Corti[c], Derek Keir[d,e]

[a] School of Earth Sciences, Addis Ababa University, Addis Ababa, Ethiopia
[b] School of Agricultural, Earth and Environmental Sciences, University of KwaZulu-Natal, Durban, South Africa
[c] CNR, Istituto di Geoscienze e Georisorse, UOS Firenze, Firenze, Italy
[d] National Oceanography Centre, University of Southampton, Southampton, UK
[e] Dipartimento di Scienze della Terra, Università degli Studi di Firenze, Florence, Italy

ARTICLE INFO

Keywords:
Main Ethiopian Rift
Strong upper crust
Friction coefficient
Shear strength
Brittle-ductile transition

ABSTRACT

We evaluate the frictional strength of seismogenic faults in the Main Ethiopian Rift (MER) by inverting the available, well-constrained earthquake focal mechanisms. The regional stress field is given by − 119.6°/77.2°, 6.2°/7.6°, and 97.5°/10.2° for trend/plunge of σ_1, σ_2 and σ_3, respectively agrees well with previous fault kinematic and focal mechanism inversions. We determine the coefficient of friction, μ, for 44 seismogenic faults by assuming the pore pressure to be at hydrostatic conditions. Slip on 36 seismogenic faults occurs with $\mu \geq 0.4$. Slip on the remaining eight faults is possible with low μ. In general, the coefficient of friction in the MER is compatible with a value of μ of 0.59 ± 0.16 (2σ standard deviation). The shear stresses range from 16 to 129 MPa, is similar to crustal shear stress observed in extensional tectonic regimes and global compilations of shear stresses from major fault zones. The maximum shear stress is observed in the ductile crust, below the seismologically determined brittle-ductile transition (BDT) zone. Below the BDT, the crust is assumed to be weak due to thermal modification and/or high pore fluid pressure. Our results indicate linearly increasing μ and shear stress with depth. We argue that in the MER upper crust is strong and deforms according to Coulomb frictional-failure criterion.

1. Introduction

Thorough understanding of the regional stress field is of paramount importance in constraining the strength of faults and the crust along actively deforming plate boundaries. In general, fault zones are relatively weaker than the surrounding stable crust (Zoback et al., 1987). However, there are still questions regarding whether the strength of individual faults in a deformed region is the same or varies, and also whether the strength of the fault varies along strike on the same fault. In a recent study, Floyd et al. (2016) showed that the frictional parameters of a fault may vary over only a few kilometers distance depending on lithological controls. Fault strength varies not only spatially but also temporally. By reviewing about 300 experimental results, Di Toro et al. (2011) suggested that the strength of faults could be reduced during earthquakes.

Coefficient of friction, μ, can be used as a proxy to model the strength of faults and crust. Laboratory estimates of μ are usually high, ranging from 0.6 to 0.8 (Byerlee, 1978) although lower μ values are reported (using rotary shear apparatus) from the San Andreas fault (e.g., Carpenter et al., 2015). Some researchers argue that if these μ values really exist during seismic slip, we should have found high heat flow and extensive melting (e.g. pseudotachilite) along exhumed faults (e.g., Mulargia and Bizzarri, 2016). The apparent absence of these rock types is used to argue that coefficient of friction is lower than laboratory estimates. In line with this, numerical modeling studies in active tectonic areas, e.g. in East African Rift (EAR) (Bird et al., 2006), argue that the friction coefficient is much lower than the laboratory estimates. This agrees with recent laboratory experiment that found μ to be below 0.4 under pressure condition equivalent to a depth of ~15 km (Di Toro et al., 2011).

Mulargia and Bizzarri (2016) proposed a multi-stage earthquake process which involves a high friction coefficient with $\mu \sim 0.7$ during the first stage. The high friction stage induces high temperature that almost immediately induces fluid pressurization and reduces the permeability of fault gouges and subsequently the pore pressure reaches lithostatic state. In this case, μ drops to ~0.2. Other, equally important fault lubrication mechanisms include melt lubrication (Di Toro et al., 2006), gelification (Di Toro et al., 2004) and decarbonation (Han et al.,

* Corresponding author.
E-mail address: ameha.atnafu@aau.edu.et (A.A. Muluneh).

https://doi.org/10.1016/j.tecto.2018.03.010
Received 26 September 2017; Received in revised form 18 February 2018; Accepted 16 March 2018
Available online 23 March 2018

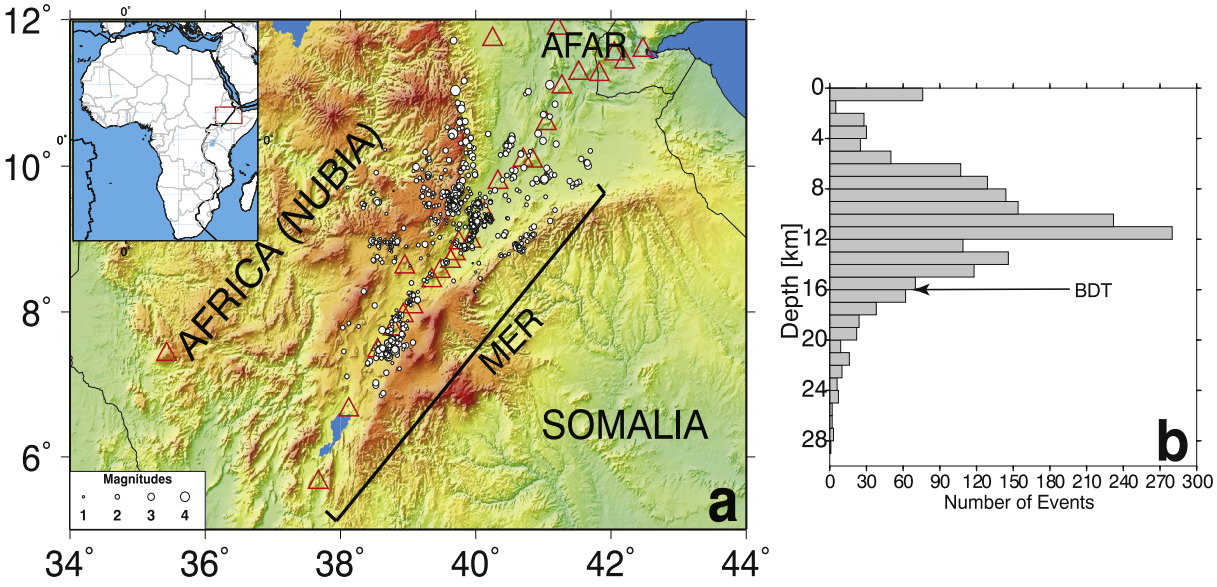

Fig. 1. Location map of the Main Ethiopian Rift (MER). (a) The main map of the study area with inset showing map of Africa. The white circles are earthquake epicenters determined by EAGLE network for a period of 2001–2003 (Keir et al., 2006). The size of the circles is scaled to their magnitudes. The red triangles are active volcanic centers. (b) Histogram of the number of earthquakes per 1 km depth bin interval. BDT shows the depth to brittle-ductile transition at 16 km where 90% of seismicity occurs. MER = Main Ethiopian Rift. (For interpretation of the references to color in this figure legend, the reader is referred to the web version of this article.)

2010), which are also proposed for the reduction of μ during seismic slip.

Stamps et al. (2015) argue that buoyancy forces, weak continental faults and Couette-type mantle flow in the asthenosphere explain extension across the EAR. In that study, weak fault friction results in better fit between geodynamic model and present-day geodetic observations in Africa (Saria et al., 2014).

In the Main Ethiopian Rift (MER) (Fig. 1), the crust and faults are assumed to be weakened by hotspot tectonics over the last ~30 Ma (e.g., Pik et al., 2006), including ongoing dyke intrusion (e.g., Keranen et al., 2009; Wright et al., 2006; Beutel et al., 2010). We constrain the coefficient of friction and stress magnitudes in the actively deforming MER. Our approach is that first we invert the focal mechanisms and follow basic assumptions of finding the shear and normal stresses using tensor transformation, acting on optimally oriented seismogenic faults and subsequently determine the coefficient of friction, μ. Our results show spatial variation of μ along the strike of the MER and the shear stress variation in the crust. The results presented will contribute to the understanding of the stress magnitude at the earthquake focal depths where in situ measurements are totally absent and the frictional strength of MER faults and crust.

2. Tectonic setting, focal mechanism data and regional stress field

2.1. Tectonics of the Main Ethiopian Rift

The Main Ethiopian Rift forms an active plate boundary between the Africa (Nubia) and Somalia plates in the northern EAR. Starting from ~18 Myrs, the MER is thought to have initiated asynchronously along its length (Wolfenden et al., 2004). The asynchronous development of the different sectors of the rift potentially influences the melt production and strain accommodation mechanisms (Keir et al., 2015; Muluneh et al., 2017). The MER orientation is influenced by the Neoproterozoic, Pan-African suture zone that runs through Ethiopia, and significantly influences the orientation of faults (e.g., Agostini et al., 2011), seismic anisotropy (e.g., Gashawbeza et al., 2004) and also crustal thickness (e.g., Keranen and Klemperer, 2008). During the past ~2 Myrs, deformation in the northern MER focused along 20 km-wide, 60 km-long magmatic segments arranged in an en echelon manner within mid-Miocene half-graben basin (Ebinger and Casey, 2001). The transfer of strain from border faults to the magmatic segments could be due to rift obliquity (Corti, 2008), weakening of the crust by release of magmatic fluids (Muirhead et al., 2016), or by localizing extensional stresses in strong crust within the rift in which the increase in the rock strength is due to metamorphic reactions in rocks intruded by ascending magmas (Lavecchia et al., 2016), and/or by solidification of new mafic material (e.g., Beutel et al., 2010).

2.2. Earthquake focal mechanism data

Earthquake data from the EAGLE catalogue (Keir et al., 2006) for the period 2001 to 2003 (Fig. 1a & b) shows that seismicity continues to the depth of 28 km with magnitude M_L 0.0 to 4 (Fig. 1a & b). We assume that the depth to the brittle-ductile transition (BDT) occurs at a depth of 16 km, above which 90% of seismicity occurs (Fig. 1b). This depth also coincides with the average depth to the base of the upper crust in the MER (Maguire et al., 2006).

We compiled 55 well determined earthquake focal mechanisms from CMT catalogues and published sources (Fig. 2a) (Ayele, 2000; Hofstetter and Beyth, 2003; Ayele et al., 2006; Keir et al., 2006; Delvaux and Barth, 2010; Wilks et al., 2016) in the MER. Fig. 2b shows hypocentral depth of the focal mechanisms compiled and only two mechanisms are located in the lower crust. The focal mechanism data are strike, dip and rake of the fault planes. Most of the studies reported the fault planes except for Hofstetter and Beyth (2003) who reported both the auxiliary and interpreted fault planes. Distinction between fault and auxiliary planes is based on orientation of fault traces on the surface. Planar faults tend to have linear fault traces on the Earth's surface whereas listric fault planes tend to be arcuate in plan view and listric in 3-D with alternating and overlapping half grabens that change polarity along strike (Rosendahl, 1987). In the MER, the observed faults on the surface are linear segments with steep fault plane that led us to conclude that they continue to be planner at depth. In cases when multiple mechanisms for a single earthquake is reported, we use the most recent publication. The largest focal mechanism dataset comes from Keir et al. (2006) (33 out of 55 mechanisms) who assign a 2 sigma

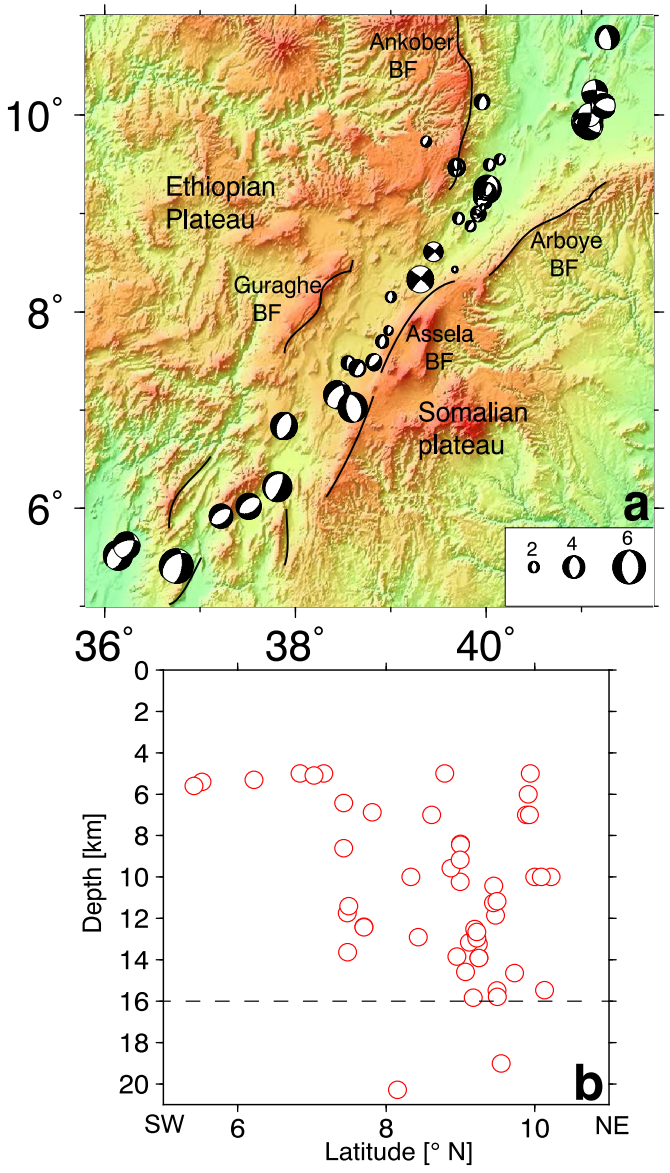

Fig. 2. (a) Earthquake focal mechanisms compiled for this study scaled to the magnitude of events. (b) Depth of earthquake focal mechanisms is shown on (a). BF = border fault.

uncertainty of ± 20° to the focal parameters and ± 2 km for the hypocentral depth. Most focal mechanisms show dip-slip movements along the faults and slip with dips > 50° similar to the dip of recently active faults in the rift (e.g., Agostini et al., 2011).

2.3. Inversion method and regional stress field

The stress field can be quantified by formally inverting a group of earthquake focal mechanisms or active fault data. A least square inversion technique is developed to invert a group of diverse earthquake mechanisms by assuming the regional stress field is uniform (Michael, 1984). The inversion technique minimizes the difference between the slip vector and the resolved shear stress which can be used to assess the success of the inversion result. The resulting stress field quantifies the relative magnitude, ϕ, trend and plunge of principal stresses (σ_1, σ_2 and σ_3; where $\sigma_1 \geq \sigma_2 \geq \sigma_3$). We used the inversion method of Michael (1984, 1987) in order to estimate the regional stress field of the MER. The confidence region for the best fit stress tensor is calculated using the bootstrap resampling method. To estimate the 95% confidence limit

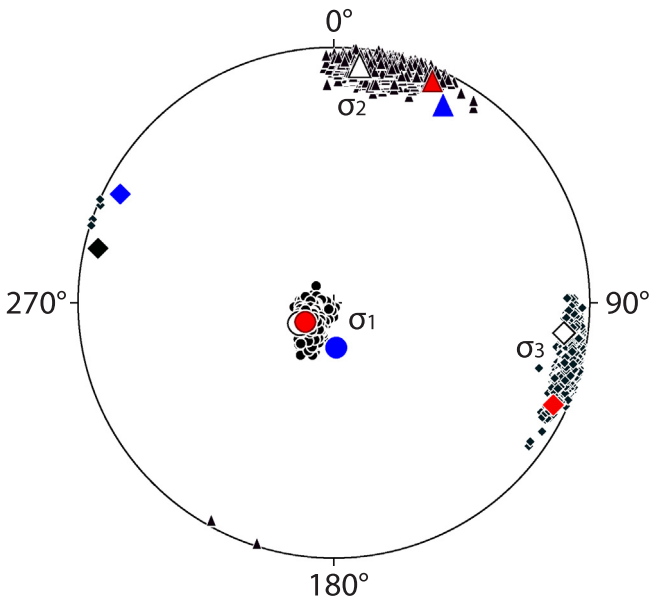

Fig. 3. Result of stress tensor inversion using earthquake focal mechanisms in the MER. Circle, triangle and diamond symbols show σ_1 (largest compressive stress), σ_2 (intermediate), and σ_3 (least compressive stress), respectively. The 95% confidence level is estimated with bootstrap resampling (Michael, 1987). Inversion results in our study are shown by open symbols. Principal stresses from Delvaux and Barth (2010) using Delvaux and Sperner (2003) are shown by blue and using Michael (1984) by red filed symbols. Black diamond symbol shows σ_3 orientation from Keir et al. (2006). (For interpretation of the references to color in this figure legend, the reader is referred to the web version of this article.)

we used 2000 repetitions (Michael, 1987). During the inversion process, we used the reported fault planes (Ayele, 2000; Ayele et al., 2006; Keir et al., 2006; Wilks et al., 2016) as they are. In cases when we encounter large angular misfit during the inversion process, we change the nodal plane until the misfit is reduced to an acceptable level. The nodal planes that reduce the angular misfit are the preferred fault planes (Michael, 1987). However, the individual misfit of each plane must be kept below 25° (Michael, 1991). Only two focal mechanisms show individual misfit of higher than 25° but below 30°. The observed regional stress field is given by − 119.6°/77.2°, 6.2°/7.6°, 97.5°/10.2° for trend/plunge of σ_1, σ_2 and σ_3 (Fig. 3; Table 1). The quality of the inversion result is measured by the β value; a misfit measure that defines the angle between the observed and predicted rake angles for the mechanisms (Michael, 1984). Our inversion results an average misfit, $\overline{\beta}$, of 10.3° ± 7.6°. Although the inversion process suffers from the absence of diverse focal mechanisms, it results in similar trend and plunge of principal stress axes to other studies in the rift (e.g., Delvaux and Barth, 2010; Keir et al., 2006) and extension direction inferred from GPS observations (e.g., Saria et al., 2013). In addition, the focal mechanism dataset is a complete compilation of literature.

Several studies have been conducted in order to compare different inversion techniques (e.g., Kastrup, 2003; Delvaux and Barth, 2010). Irrespective of the methods used, the optimal solutions for the stress inversion are consistent and similar. Using 7 earthquake focal mechanism solutions from CMT catalogue in the MER, Delvaux and Barth (2010) conducted stress inversions using the method of Michael (1984, 1987) and Delvaux and Sperner (2003). They showed that the orientation of the principal stress axes is almost the same with significant difference in stress ratio.

2.4. Absolute stress magnitudes

In areas where in-situ stress measurements are lacking, a number of

Table 1
Stress inversion results from earthquake focal mechanism data.

# of fms	σ_1 tr/pl [°]	σ_2 tr/pl [°]	σ_3 tr/pl [°]	$\bar{\beta}$ ± s.d. [°]	$\bar{\tau}$ ± s.d. [°]	ϕ	Reference
44	−119.6/77.2	6.2/7.6	97.5/10.2	10.3 ± 7.6	0.93 ± 0.2	0.37	This study
7	178/76	029/13	297/07	–	–	0.57	DB10
7	239/79	024/09	115/06	–	0.94 ± 0.19	0.79	DB10*
36	–	–	283/06	10.9 ± 7.0	–	–	D06

# of fms = number of focal mechanism solutions; tr/pl - trend/plunge of the principal stress axes; ϕ measures the relative size of principal stresses. $\bar{\tau}$ ± s.d. - the average angular misfit with standard deviation. High standard deviation might be due to a non-diverse range of focal mechanisms (Keir et al., 2006). fms = focal mechanism solutions, DB10* = Delvaux and Barth (2010) using Michael (1984) method, DB10 = Delvaux and Barth (2010) using Delvaux and Sperner (2003) method; D06 = Keir et al. (2006).

assumptions can be used to find the absolute magnitude of principal stresses at the earthquake focal depths and later used to quantify the strength of the crust. In order to quantify the shear and normal stresses and later the coefficient of friction, μ, on optimally oriented faults, information about the absolute magnitude of the principal stresses is required (Zoback, 1992). Earthquake focal mechanism inversion allows the determination of direction and relative magnitudes of principal stresses, σ_1, σ_2, and σ_3. When one principal stress axis is oriented vertically (σ_1 in extensional regime), its magnitude is given by the overburden weight (e.g., Zoback and Zoback, 2002)

$$\sigma_v = \sigma_1 = \int_0^z \rho g dz \approx \rho g z \tag{1}$$

where ρ is the density of crustal material (taken here as 2800 kg/m^3), g is acceleration due to gravity [~10 m/s^2] and z is the focal depth [m]. Eq. (1) shows that σ_1 increases in an approximately a linear fashion with depth.

Based on limiting frictional strength of optimally oriented faults in the crust (e.g., Sibson, 1974; Zoback and Townend, 2001), the least compressive stress, σ_3, can be estimated by

$$\frac{\sigma_1 - p_0}{\sigma_3 - p_0} = [(\mu_c^2 + 1)^{1/2} + \mu_c]^2 \tag{2}$$

where p_0 is the pore fluid pressure which is assumed to be hydrostatic and is given by $\lambda \times \sigma_v$ where $\lambda = 0.3737$ (Albaric et al., 2009; Zoback, 1992; Fadaie and Ranalli, 1990); μ_c is a static frictional coefficient ~0.75 (Sibson, 1974; Jager and Cook, 1979) and is considered to represent the regional value for absolute stress determination (Kastrup, 2003). From Eq. (2), it is evident that p_0 can not exceed σ_3 without the occurrence of hydraulic fracturing, although λ values greater than 1 are possible without causing hydraulic fracturing if total principal stresses within the fault zone are magnified due to contrasts in rheological properties (e.g., Rice, 1992). Inserting the μ_c value into $\theta = \frac{1}{2}\tan^{-1}\left(\frac{1}{\mu_c}\right)$, where θ is the angle σ_1 makes with the fault plane, gives the dip angle of ~ 63° for optimally oriented normal faults (Sibson, 1974). This angle is the typical dip of normal faults (Agostini et al., 2011) and the interpreted fault planes of earthquake focal mechanisms (Keir et al., 2006) (Fig. 4a & b) in the MER. Fig. 3 shows that σ_1 is near-vertical and fulfills the assumption of vertical maximum stress in order to determine absolute stress magnitude.

Finally an additional constraint to the determination of absolute magnitudes is given by

$$\phi = \frac{\sigma_2 - \sigma_3}{\sigma_1 - \sigma_3} \tag{3}$$

in which ϕ value is independently determined from the inversion of earthquake focal mechanisms. Eqs. (1)–(3) are adequate to estimate the absolute magnitude of principal stresses.

To get the normal (σ_n) and shear (τ) stresses on individual fault plane, we need to transform the stress tensor through tensor transformation (e.g., Allmendinger et al., 2012). To quantify the frictional strength of the faults, the ratio of τ to $\dot{\sigma_n}$ must be determined using the modified linear frictional sliding equation (Eq. (4)) where the cohesion is assumed to be close to zero (Zoback, 1992, and references therein)

$$\tau = \mu(\sigma_n - p_0) = \mu\dot{\sigma_n} \tag{4}$$

where μ is considered to represent the frictional strength of the earthquake faults. We assume that the pore pressure to be hydrostatic and we vary μ to match the normal and shear stresses.

3. Results and discussion

3.1. Coefficient of friction, μ

The ratio of shear to effective normal stresses give μ values on each fault (Fig. 5). Fig. 6a & b shows μ values plotted in the MER. We estimated the frictional parameters (μ, normal and shear stresses) for 44 well constrained earthquake focal mechanisms in the MER. Earthquakes used in the this study together with calculated σ_n, τ and μ are included as a supplementary material to this paper.

Most faults in the MER fail under high frictional stress with $\mu \geq 0.3$. A regression of all the μ values (Fig. 5) indicates the rift deforms according to laboratory-determined friction coefficients (Byerlee, 1978). The average value for the crust is computed using $\frac{\sum_{i=1}^{N}\mu_i f_i}{\sum_{i=1}^{N} f_i}$ from distribution of μ values on earthquake faults, where μ_i and f_i are friction coefficients and number of events, respectively. In general, the crust fails with μ of 0.59 ± 0.16 (2σ standard deviation). Box plot of μ values (Fig. 5) also fall within this range.

An exception to the relatively high μ values for most of the data, is that six focal mechanisms have μ ranging from 0.21 to 0.3 (Fig. 7a). There are potentially several explanations for the low μ results. We observed a cluster of 3 earthquakes near the axis of the northernmost MER with $\mu < 0.3$ (Fig. 7a). These earthquakes are spatially and temporally coincident with the intrusion of a dyke near Amoissa volcano during May 2000, and interpreted to be induced by stress change above the new intrusion (Keir et al., 2011). Two strike-slip faults of M_L 1.4 and 1.55 beneath Fentale volcano make angles of 64° and 56° to σ_H, higher than the angle expected for reactivated strike-slip faults, and as a result slip with μ of 0.23 and 0.3, respectively. Weak faults such as the San Andreas Fault fail by creeping with small magnitude earthquakes (M_w ~ 2) (Nadeau and Guilhem, 2009). The low frictional strength and low magnitude earthquakes might explain failure by creeping along the two strike-slip faults.

An additional focal mechanism (Keir et al., 2006) with a selected nodal plane with a dip of 22° (selected during the inversion since this lowers the individual misfit to 6.8°) shows a μ of 0.21. The new dip angle deviates by ~40° from optimally oriented normal faults (Fig. 4b) so that a lower μ is evident. Traditionally, normal faults with dip angle of < 30° were not thought to be able to lock and subsequently slip as earthquakes (Collettini et al., 2011), but emerging evidence of slip on low angle normal faults, e.g. in West Salton detachment faults (Prante et al., 2014) argues that low angle fault might slip through earthquakes. The geometry of this fault can be explained by very low μ, near

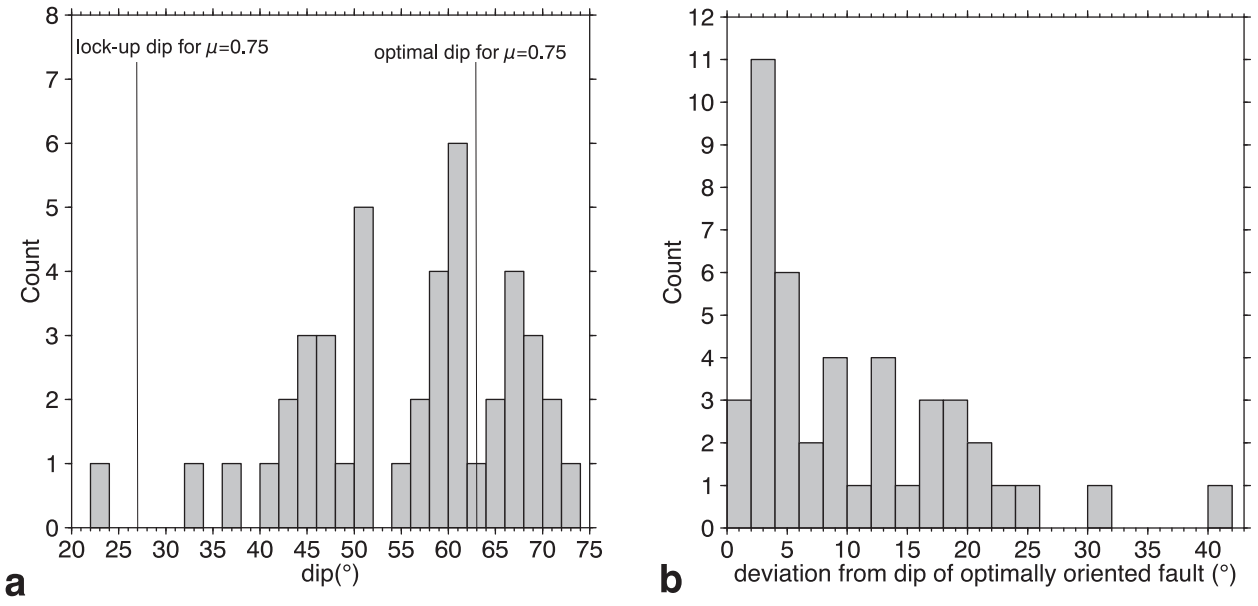

Fig. 4. (a) Histogram of the dips of focal mechanisms with unambiguously determined fault planes per 2° bin. (b) Deviation of the dip angles from optimal dip of fault for $\mu = 0.75$. Lock-up angle of fault planes, 27° for $\mu = 0.75$ is also shown. All, but one, fault planes are above the expected angle of ~30° for reactivation of normal faults.

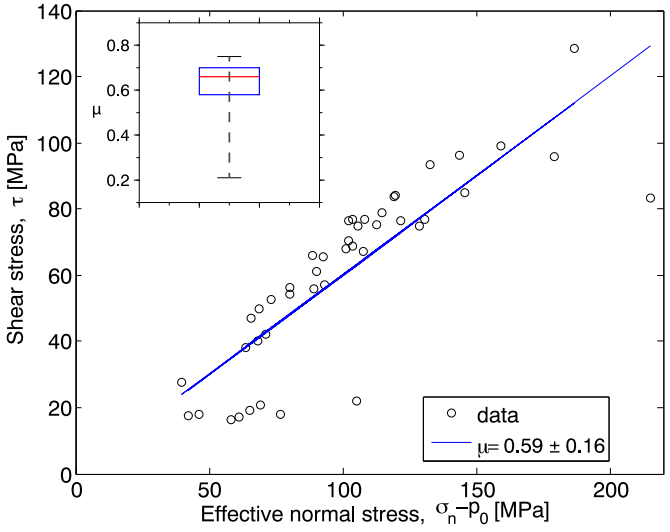

Fig. 5. Shear stress vs effective normal stress plot to estimate the coefficient of friction, μ on each earthquake fault (circles). A linear fit in the main map defines $\mu = 0.59 \pm 0.16$ (2σ standard deviation). A Tucky box plot in the inset shows a median value of 0.66 and the box outlines the upper and lower quartiles of 0.7 and 0.58, respectively.

lithostatic pore pressure or some combination of the two. Middleton and Copley (2013) noted that slip on such low angle normal faults possibly occurs due to the presence of weak materials along the pre-existing fault surface. Lower strength faults at shallower depth could be due to the presence of clay minerals along the fault surfaces and high temperatures near active magmatic centers, such as beneath Fentale and Amoissa volcanoes (e.g., Keir et al., 2011).

The estimated μ for one mechanism at a depth of ~19 km is ~0.67 (Fig. 7a). The shear stress for the same mechanism is ~70 MPa (Fig. 7b), lower than the maximum shear stress observed at the BDT (~100 MPa) (Fig. 7b). In order for a slip to occur at higher μ and lower shear stress, the effective normal stress should be low which in turn implies higher pore pressure at this depth. This hints that the pore pressure in the lower crust might be in super hydrostatic or lithostatic condition.

Plotting the distribution of μ with depth (Fig. 7a) indicates that μ generally increases upwards from the BDT. Below the BDT, μ decreases from the maximum value but is still high (0.65–0.7). Fig. 7a shows μ values cluster in two zones. At 0–10 km depth, the crust is mainly characterized by μ of 0.2–0.4. Below 10 km up to 16 km, the crust is generally characterized by higher μ (~0.6–0.75). The high μ (~0.6) observed for MER faults is also supported by the agreement between P-, B-, and T-axes of the earthquake focal mechanisms and the regional stress field (e.g., Keir et al., 2006). Zoback and Zoback (2002) argue that in regions for which μ ranges from 0.6 to 1, P-, B-, and T-axes approximate the average principal stress orientations.

Our estimate of μ for the MER crust deviates significantly from the frictional parameter inferred using numerical modeling studies in the EAR (Bird et al., 2006; Stamps et al., 2015). To produce a better fit with observed plate scale separation of Somalia from Africa, low fault friction is required (Bird et al., 2006; Stamps et al., 2015). We argue that discrepancy between our results and numerical modeling studies might be due to the input and model parameters used in the numerical modeling studies.

3.2. Frictional strength of the crust

Maggi et al. (2000) questioned the popular view of continental strength profiles in which a weaker lower crust resides between stronger upper crust and mantle. Spatial variation in continental strength of the lithosphere is mainly controlled by the presence or absence of smaller amounts of water (Maggi et al., 2000). Topography and gravity field analysis indicate that lithospheric stress is supported by upper crust overlying a weaker lower crust (Thatcher and Pollitz, 2008).

Albaric et al. (2009) noted that the strength of lithosphere/crust can vary within the same tectonic setting. Even on a finer scale, Floyd et al. (2016) showed how the along strike variation of rheological properties controls the frictional strength of a fault. Here we discuss the frictional strength of the MER crust based on shear stress magnitudes estimated at hypocentral depth. The shear stress magnitude varies from 16.2 to 129 MPa with an average value of 60 MPa similar to crustal-average shear stress of 56 MPa (e.g., Bird, 1999). Similar to μ values, the shear

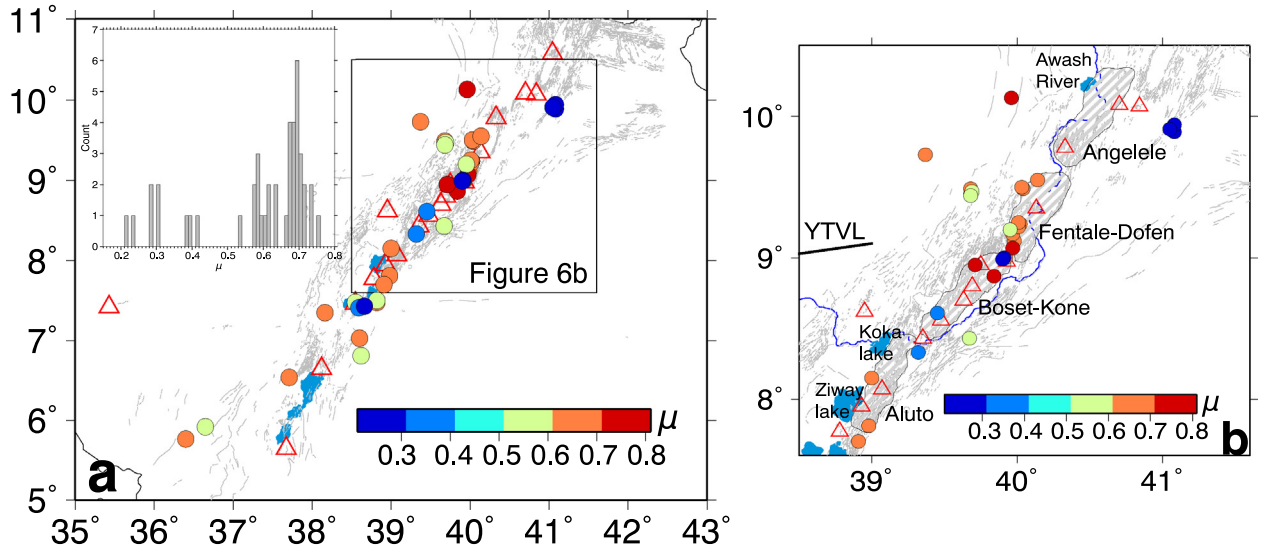

Fig. 6. (a) Variation of μ values in the MER. Inset shows the histogram of μ values. (b) Zoom in of the open rectangle in (a) with tectono-magmatic segments shown by gray filled area (Wolfenden et al., 2004). The magmatic segments are characterized by higher μ (≥ 0.4) which could be due to melt-induced thermal metamorphism as shown by Lavecchia et al. (2016). However, low μ values are observed at or near active volcanic centers (red triangles). YTVL = Yerrer-Tullu Wellel Volcano-tectonic Lineament. (For interpretation of the references to color in this figure legend, the reader is referred to the web version of this article.)

stress also show a lower value (~20 MPa) above 10 km and ranges from 40 to 100 MPa between 10 and 16 km. One earthquake fault fails with a shear stress of 129 MPa (Fig. 7b), at ~20 km depth, higher than friction controlled shear stress for the upper crust.

The shear stress variation with depth seems inconsistent with models in which significant decrease in strength occurs at the BDT (e.g., Chester, 1995) but rather shows an increase to a depth of ~20 km, within the ductile, lower crust. This argument, however, is based on only one focal mechanism. A recent thermo-mechanical modeling study in the MER (Lavecchia et al., 2016) shows a transition from brittle to ductile rheology at a depth between 20 km and 25 km. On the other hand, geophysical studies show that the lower crust is weak (Keranen et al., 2009) and therefore the highest shear stress observed here might be due to the hydrostatic pore pressure imposed in our calculation.

Fig. 7b shows that faults at depths shallower than the 10 km appear to be weaker than their equivalent at depth below 10 km. This agrees with the global compilation of stress-depth data (Behr and Platt, 2014) that middle crust sustains higher stress than the brittle faults above. Furthermore, the process that allows slip at lower shear stress (~16–50 MPa, Fig. 7b) in the brittle crust terminates at 10 km depth probably due to higher temperature in the lower part of the upper crust.

Our argument for strong crust and faults in the MER agrees well with the modeling studies in the region (Lavecchia et al., 2016; Beutel et al., 2010). Lavecchia et al. (2016) showed that the variations in mineral assemblages due to temperature increase during dyke intrusion and subsequent metamorphism locally increases the strength of the crust. This mainly occurs by changing weak minerals to strong minerals (Lavecchia et al., 2016). This agrees with the modeling results of Beutel et al. (2010) who noted an increase in the strength of the crust due to solidified mafic intrusions beneath magmatic segments. In regions of active magmatism and dyke intrusion where magma input is likely to be particularly high (i.e. near active volcanic centers), the crust appears to

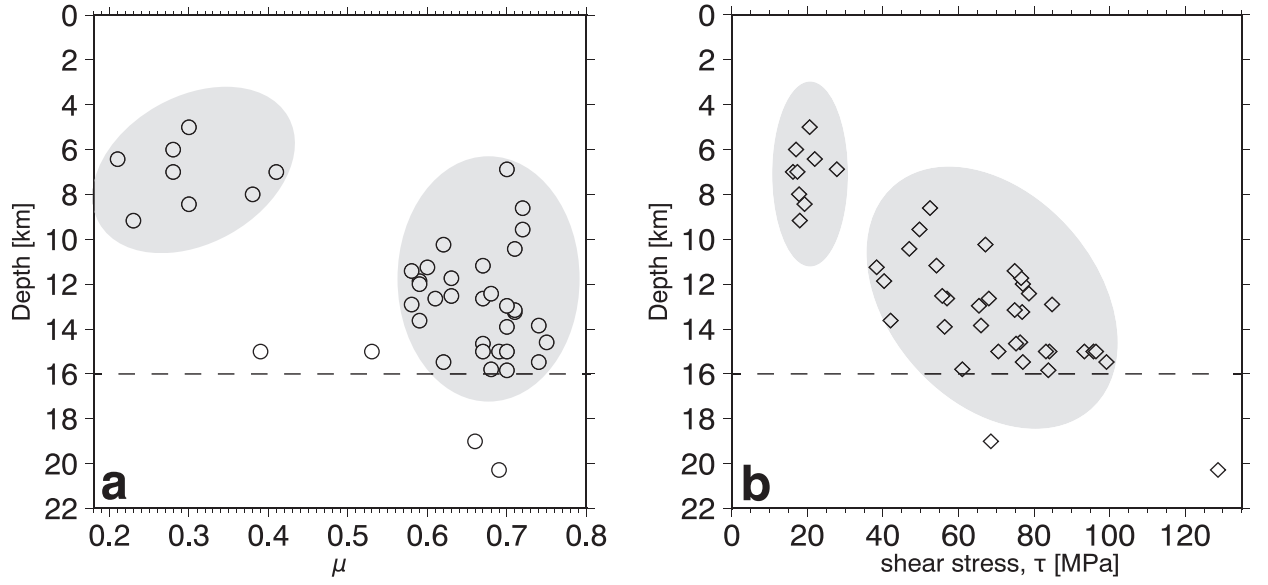

Fig. 7. (a) Coefficient of friction and (b) shear stress magnitudes plotted at hypocentral depth. The gray shaded regions show where μ (a) and shear stress (b) cluster. Both parameters show sharp increase at a depth of 10 km. The dashed line at 16 km marks the BDT.

be weak as shown by lower μ values (Fig. 6b) in agreement with modeling studies in the EAR (e.g., Bialas et al., 2010; Daniels et al., 2014).

The strong faults and crust inferred in our study directly influence kinematics of crustal blocks in the MER. Recent GPS study from EAR (e.g., Saria et al., 2014) shows significant deviation in Nubia-Somalia motion from the stable parts of the plates and crustal blocks in the MER. This points to argument that strength of the faults and crust controls the surface kinematics of the MER.

Strength of the faults and the crust are very sensitive to the pore fluid pressure considered (Sibson, 2000). Elevated pore pressures change the state of effective stress and reduce the force required for deformation to occur (Hubbert and Rubey, 1959). An experiment on fluid-rock interaction (Reynolds and Lister, 1987) showed existence of high fluid pressure in the ductile part of the crust. For the EAR, high pore pressure due to dehydration of metamorphic minerals in the lower crust is invoked (Seno and Saito, 1994). However, Keir et al. (2009) argued that in the absence of any accumulated fluid in the lower crust, earthquake activities are controlled by emplacement of melt supplied from the upper mantle into the lower crust. This argument is in line with geochemical evidence of water-poor magmas in the lower crust (Rooney et al., 2005). High pore fluid pressure and hence low strength of faults and of the crust makes a number of predictions (e.g., Scholz, 2000) including a low magnitude of shear stress and high angle between σ_1 and the fault plane. Although, there are no reported measurements on the magnitude of shear stress in MER, structural mapping on active faults and studying earthquake focal mechanisms show that σ_1 forms a low angle with the fault planes. The latter lends support to the interpretation that the faults in the rift are strong.

3.3. Hydrostatic vs lithostatic pore pressure

Pore fluid pressure is the most uncertain parameter in the calculation of the strength profile of the crust (e.g., Brace and Kohlstedt, 1980). Constraints on pore pressure in the MER are scarce. In order to assume the pore pressure is near lithostatic state, either the rock permeability must be very low (Nur and Walder, 1990) or an active source of overpressured fluids must exist at depth (Rice, 1992). Townend and Zoback (2000) and Barton et al. (1995) showed that critically stressed faults are hydraulically conductive and act like fluid conduits. These faults control the permeability of the crust and results in short diffusion time (10–1000 years over distances of 1–10 km). In extensional tectonic setting of the Taupo volcanic zone, high permeability ($k > 10^{-16}$) causes earthquake ruptures (Sibson and Rowland, 2003). This implies that fluid pressures in the crust equilibrate over relatively shorter time and hydrostatic pore pressure develops within the crust. Note that long diffusion time ($> 10^5$ years) leads to near-lithostatic pore pressure to be maintained (Nur and Walder, 1990).

In the previous sections, we showed that the MER faults are favorably oriented and hence facilitate the easy passage of fluids and supports the notion that the pore pressure in the region is near hydrostatic state. Recent CO_2 degassing study at Aluto volcano in the central MER estimated a total of 250–500 t d^{-1} CO_2 emitted along major faults and volcanic structures (Hutchison et al., 2015). Such emission rate is comparable to rates observed in the Eastern rift of the EARS (Lee et al., 2016). Furthermore, maximum CO_2 flux is observed adjacent to the faults implying that the permeability of faults in the MER is high and gives an easy access to the flow of fluids. Hutchison et al. (2015) also noted that the faults in the Aluto volcano penetrate deep and connect the reservoir to the surface. This provides a favorable condition for the fluid to reach hydrostatic state in a relatively short time period. Permeability values ranging 0.5–1.1 $\times 10^{-12}$ m^2 are estimated from ~2 km deep Aluto-Langano geothermal wells (Electroconsult, 1985). Deep penetrating faults in other parts of the EAR (e.g. in Tanzania) are known to act as pathways for CO_2 ascent (e.g., Lee et al., 2016). Seismicity recorded by CRAFTI array suggest that volatiles migrate from upper mantle or lower crust following extensional faults (e.g., Lee et al., 2016). However, it is questionable whether the permeability at upper crustal level is adequately representative of the deeper level or not (Sibson, 2000). Recent geophysical studies in the EAR (Lindenfeld et al., 2012; Weinstein et al., 2017) and Taupo rift (Reyners et al., 2007) showed that high pore fluid pressure induce faulting and seismic activities in the lower crust. Geophysical studies in MER (Keranen et al., 2009) and Tanzanian rift (Weinstein et al., 2017) indicated that the lower crust in these regions is weak and ductile and higher pore fluid pressure can provide a mechanism for brittle failure at lower shear stress. Our compilation of earthquake focal mechanisms in MER indicated that only two earthquake focal mechanisms occurred in the lower crust (below 16 km). For the two lower crustal earthquake focal mechanisms, we examine how increased pore pressure (from hydrostatic to super hydrostatic; i.e. 0.56 $\times$ σ_v) affects the strength of the faults. Using a mean μ of 0.59 and normal stress values (see the supplementary material), Eq. (4) results in the shear stress of 34 MPa and 3 MPa for focal mechanisms at depths of 20.29 km and 19.01 km, respectively. Increasing the pore pressure from hydrostatic to super hydrostatic conditions leads to significant reduction of shear strength of earthquake faults.

However, since most of focal mechanisms occur at depths above 16 km, the assumption of hydrostatic pore pressure can be considered as adequately representative of the state of pore fluid pressure in the upper crust and well depicts the strength of the crust and faults in the MER. We found both high and low μ values for earthquake faults in the MER implying that thermal modifications are more important than pore fluid pressure in modifying the strength of the faults in the upper crust.

Finally, further studies constraining the condition of pore fluid pressure in the crust are required in order to link fluid weakening and deep crustal earthquakes in MER.

4. Conclusions

Based on our findings, we reach the following conclusions:

1. Based on the orientation of optimally oriented faults controlling the flow of fluids in the rift and high CO_2 seepage rate, we argue that pore pressure in the upper crust is in near hydrostatic state. However the argument for hydrostatic pore pressure in the lower crust might be flawed as indicated by high μ, low shear strength fault and deep crustal seismicity.
2. Very low μ (≤ 0.3) values are observed near active volcanic centers, whereas high μ correspond to areas either at margins or in between magmatic segments implying that high pore fluid pressure might not be required for slip on weak faults.
3. Although data from the southern MER are scarce, there are no indications of weak faults, which could be in agreement with a less evolved rifting and lower magmatic modification in the area.
4. A best fit of μ values for MER faults indicate a regional value of 0.59 ± 0.16 implying the crust is strong under hydrostatic condition.
5. The strong upper crust contributes to the strength of the lithosphere in the MER, with the lower portion of the upper crust (10–16 km) being the strongest layer.

The strong faults and crust inferred in our study directly influence the kinematics of crustal blocks in the MER. Therefore, the conclusion we draw can be tested by future geodetic and modeling studies.

Acknowledgments

AM and TK acknowledge the support from NAS through GeoPower Africa project sub-grant 2000004834. DK is supported by NERC grant NE/L013932/1. The manuscript benefited from detailed and constructive reviews by Damien Delvaux and an anonymous reviewer. We

also thank Prof. Jean-Philippe Avouac for his comments and editorial handling. The figures were drafted with Generic Mapping Tools (Wessel and Smith, 1998).

Appendix A. Supplementary data

Supplementary data to this article can be found online at https://doi.org/10.1016/j.tecto.2018.03.010.

References

Agostini, A., Bonini, M., Corti, G., Sani, F., Manetti, P., 2011. Distribution of Quaternary deformation in the central Main Ethiopian Rift, East Africa. Tectonics 30. http://dx.doi.org/10.1029/2010TC002833.

Albaric, J., Deverchere, J., Petit, C., Perrot, J., Le Gall, B., 2009. Crustal rheology and depth distribution of earthquakes: insights from the central and southern east African Rift System. Tectonophysics 468, 28–41.

Allmendinger, R., Cardozo, N., Fisher, D.M., 2012. Structural Geology Algorithms-Vectors and Tensors, First edition. Cambridge University Press.

Ayele, A., 2000. Normal left-oblique fault mechanisms as indication of sinistral deformation between the Nubia and Somalia plates in the Main Ethiopian Rift. J. Afr. Earth Sci. 31, 359–368.

Ayele, A., Nyblade, A., Langston, C., Cara, M., Leveque, J., 2006. New evidence for Afro-arabian plate separation in southern Afar. In: Yirgu, G., Ebinger, C., Maguire, P.K.H. (Eds.), The Afar Volcanic Province Within the East African Rift System. 259. Geological Society of London, pp. 133–141.

Barton, C., Zoback, M.D., Moos, D., 1995. Fluid flow along potentially active faults in crystalline rock. Geology 23, 683–686.

Behr, W.M., Platt, J.P., 2014. Brittle faults are weak, yet the ductile middle crust is strong: implications for lithospheric mechanics. Geophys. Res. Lett. 41. http://dx.doi.org/10.1002/2014GL061349.

Beutel, E., van Wijk, J., Ebinger, C., Keir, D., Agostini, A., 2010. Formation and stability of magmatic segments in the Main Ethiopian and Afar rifts. Earth Planet. Sci. Lett. 293. http://dx.doi.org/10.1016/j.epsl.2010.02.006.

Bialas, R.W., Buck, W.R., Qin, R., 2010. How much magma is required to rift a continent? Earth Planet. Sci. Lett. 292, 68–78.

Bird, P., 1999. Thin-plate and thin-shell finite-element programs for forward dynamic modeling of plate deformation and faulting. Comput. Geosci. 25, 383–394.

Bird, P., Ben-Avraham, Z., Schubert, G., Andreoli, M., Viola, G., 2006. Patterns of stress and strain rate in southern Africa. J. Geophys. Res. 111. http://dx.doi.org/10.1029/2005JB003882.

Brace, W.F., Kohlstedt, D.L., 1980. Limits on lithospheric stress imposed by laboratory experiments. J. Geophys. Res. 85, 6248–6252.

Byerlee, J.D., 1978. Friction of rock. Pure Appl. Geophys. 116, 615–626.

Carpenter, B.M., Saffer, D.M., Marone, C., 2015. Frictional properties of the active San Andreas Fault at SAFOD: implications for fault strength and slip behavior. J. Geophys. Res. Solid Earth 120, 5273–5289.

Chester, F.M., 1995. A rheologic model for wet crust applied to strike-slip faults. J. Geophys. Res. 100, 13,033–13,044.

Collettini, C., Niemeijer, A., Viti, C., Smith, S.A.F., Marone, C., 2011. Fault structure, frictional properties and mixed-mode fault slip behaviour. Earth Planet. Sci. Lett. 311. http://dx.doi.org/10.1016/j.epsl.2011.09.020.

Corti, G., 2008. Control of rift obliquity on the evolution and segmentation of the Main Ethiopian Rift. Nat. Geosci. 1, 258–262.

Daniels, K.A., Bastow, I.D., Keir, D., Sparks, R.S.J., Menand, T., 2014. Thermal models of dyke intrusion during development of continent-ocean transition. Earth Planet. Sci. Lett. 385, 145–153.

Delvaux, D., Barth, A., 2010. African stress pattern from formal inversion of focal mechanism data. Tectonophysics 482, 105–128.

Delvaux, D., Sperner, B., 2003. Stress tensor inversion from fault kinematic indicators and focal mechanism data: the TENSOR program. In: Nieuwland, D. (Ed.), New Insights Into Structural Interpretation and Modelling. 212. Geological Society of London Special Publication, pp. 75–100.

Di Toro, G., Goldsby, D.L., Tullis, T.E., 2004. Friction falls towards zero in quartz rock as slip velocity approaches seismic rates. Nature 427, 436–439.

Di Toro, G., Han, R., Hirose, T., De Paola, N., Mizoguchi, K., Ferri, F., Cocco, M., Shimamoto, T., 2011. Fault lubrication during earthquakes. Nature 471, 494–498.

Di Toro, G., Hirose, T., Nielsen, S., Pennacchioni, G., Shimamoto, T., 2006. Natural and experimental evidence of melt lubrication of faults during earthquakes. Science 311, 647–649.

Ebinger, C., Casey, M., 2001. Continental breakup in magmatic province. Geology 29, 527–530.

Electroconsult, 1985. Measurements and tests on Langano-Aluto deep exploratory wells. Final Report.

Fadaie, K., Ranalli, G., 1990. Rheology of the lithosphere in the East African Rift System. Geophys. J. Int. 102, 445–453.

Floyd, M.A., Walters, R.J., Elliott, J.R., Funning, G.J., Svarc, J.L., Murray, J.R., Hooper, A.J., Larson, Y., Marinkovic, P., Burgmann, R., Johanson, I.A., Wright, T.J., 2016. Spatial variations in fault friction related to lithology from rupture and afterslip of the 2014 South Napa, California, earthquake. Geophys. Res. Lett. 43. http://dx.doi.org/10.1002/2016GL069428.

Gashawbeza, E., Klemperer, S., Nyblade, A., Walker, K., Keranen, K., 2004. Shear wave splitting in Ethiopia: Precambrian mantle anisotropy locally modified by Neogene rifting. Geophys. Res. Lett. 31. http://dx.doi.org/10.1029/2004GL020471.

Han, R., Hirose, T., Shimamoto, T., 2010. Strong velocity weakening and powder lubrication of simulated carbonate faults at seismic slip rates. J. Geophys. Res. 115 (B3), B03412.

Hofstetter, R., Beyth, M., 2003. The Afar depression: interpretation of the 1960–2000 earthquakes. Geophys. J. Int. 155, 715–732.

Hubbert, M.K., Rubey, W.W., 1959. Role of fluid pressure in the mechanics of overthrust faulting. Geol. Soc. Am. Bull. 70, 115–205.

Hutchison, W., Mather, T.A., Pyle, D.M., Biggs, J., Yirgu, G., 2015. Structural controls on fluid pathways in an active rift system: a case study of the Aluto volcanic complex. Geosphere 11. http://dx.doi.org/10.1130/GES01119.1.

Jager, J.C., Cook, N.G.W., 1979. Fundamentals of Rock Mechanics, 3rd edition. Chapman and Hall, New York.

Kastrup, U., 2003. Seismotectonics and Stress Field Variations in Switzerland. Ph.D thesis. Swiss Federal Institute of Technology Zurich.

Keir, D., Bastow, I.D., Corti, G., Mazzarini, F., Rooney, T.O., 2015. The origin of along-rift variations in faulting and magmatism in the Ethiopian Rift. Tectonics 34. http://dx.doi.org/10.1002/2014TC003698.

Keir, D., Bastow, I.D., Whaler, K.A., Daly, E., Cornwell, D.G., Hautot, S., 2009. Lower crustal earthquakes near the Ethiopian rift induced by magmatic processes. Geochem. Geophys. Geosyst. 10. http://dx.doi.org/10.1029/2009GC002382.

Keir, D., Ebinger, C., Stuart, G., Daly, E., Ayele, A., 2006. Strain accommodation by magmatism and faulting as rifting proceeds to breakup: seismicity of the northern Ethiopian Rift. J. Geophys. Res 111. http://dx.doi.org/10.1029/2005jb003748.

Keir, D., Pagli, C., Bastow, I., Ayele, A., 2011. The magma-assisted removal of Arabia in Afar: evidence from dike injection in the Ethiopian Rift captured by using InSAR and seismicity. Tectonics 30. http://dx.doi.org/10.1029/2010TC002785.

Keranen, K., Klemperer, S., 2008. Discontinuous and diachronous evolution of the Main Ethiopian Rift: implications for development of continental rifts. Earth Planet. Sci. Lett. 265, 96–111.

Keranen, K., Klemperer, S., Julia, J., Lawrence, J., Nyblade, A., 2009. Low lower crustal velocity across Ethiopia: is the Main Ethiopian Rift a narrow rift in a hot carton? Geochem. Geophys. Geosyst. 10. http://dx.doi.org/10.1029/2008GC002293.

Lavecchia, A., Beekman, F., Clark, S.R., Cloetingh, S.A.P.L., 2016. Thermo-rheological aspects of crustal evolution during continental breakup and melt intrusion: the main Ethiopian Rift, East Africa. Tectonophysics 686, 51–62.

Lee, H., Muirhead, J.D., Fischer, T.P., Ebinger, C.J., Kattenhorn, S.A., Sharp, Z.D., Kinaji, G., 2016. Massive and prolonged deep carbon emissions associated with continental rifting. Nature. http://dx.doi.org/10.1038/NGEO2622.

Lindenfeld, M., Rümpker, G., Link, K., Koehn, D., Batte, A., 2012. Fluid-triggered earthquake swarms in the Rwenzori region, East African Rift - evidence for rift initiation. Tectonophysics 566, 95–104.

Maggi, A., Jackson, J.A., McKenzie, D., Priestly, K., 2000. Earthquake focal depths, effective elastic thickness, and the strength of the continental lithosphere. Geology 28, 495–498.

Maguire, P.K.H., Keller, G.R., Klemperer, S.L., Mackenzie, G.D., Keranen, K., Harder, S., O'Reilly, B., Thybo, H., Asfaw, L., Khan, M.A., Amha, M., 2006. Crustal structure of the northern Main Ethiopian Rift from the EAGLE controlled-source surveys; a snapshot of incipient lithospheric break-up. In: Yirgu, G., Ebinger, C., Maguire, P.K.H. (Eds.), The Afar Volcanic Province Within the East African Rift System. 259. Geological Society of London, pp. 269–291.

Micheal, A.J., 1984. Determination of stress from slip data: faults and folds. J. Geophys. Res. 89, 11,517–11,526.

Micheal, A.J., 1987. Use of focal mechanisms to determine stress: a control study. J. Geophys. Res. 92, 357–368.

Micheal, A.J., 1991. Spatial variations in stress within the 1987 Whittier Narrows, California, aftershock sequence: new techniques and results. J. Geophys. Res. 96, 6303–6319.

Middleton, T.A., Copley, A., 2013. Constraining fault friction by re-examining earthquake nodal plane dips. Geophys. J. Int. http://dx.doi.org/10.1093/gji/ggt427.

Mulargia, F., Bizzarri, A., 2016. Earthquake friction. Phys. Earth Planet. Inter. 261, 118–123.

Muluneh, A., Cuffaro, M., Kidane, T., 2017. Along-strike variation in deformation style inferred from kinematic reconstruction and strain rate analysis: a case study of the Ethiopian Rift. Phys. Earth Planet. Inter. 270, 176–182. http://dx.doi.org/10.1016/j.pepi.2017.07.009.

Muirhead, J.D., Kattenhorn, S.A., Lee, H., Mana, S., Turrin, B.D., Fischer, T.P., Kianji, G., Dindi, E., Stamps, D.S., 2016. Evolution of upper crustal faulting assisted by magmatic volatile release during early-stage continental rift development in the East African Rift. Geosphere 12, 1670–1700.

Nadeau, R.M., Guilhem, A., 2009. Nonvolcanic tremor evolution and the San Simeon and Parkfield, California, earthquakes. Science 325. http://dx.doi.org/10.1126/science.1174155.

Nur, A., Walder, J., 1990. Time-dependent hydraulics of the earth's crust. In: Bredehoeft, J.D., Norton, D.L. (Eds.), The Role of Fluids in Crustal Processes. 113–127 National Academy Press, Washington, DC.

Pik, R., Marty, B., Hilton, D.R., 2006. How many mantle plumes in Africa? The geochemical point of view. Chem. Geol. 226, 100–114.

Prante, M.R., Evans, J.P., Janecke, S.U., Steely, A., 2014. Evidence for paleoseismic slip on a continental low-angle normal fault: tectonic pseudotachylyte from the West Salton detachment fault. Earth Planet. Sci. Lett. 387, 170–183.

Reyners, M., Eberhart-Phillips, D., Stuart, G., 2007. The role of fluids in lower-crustal earthquakes near continental rifts. Nature 446, 1075–1078.

Reynolds, S.J., Lister, G.S., 1987. Structural aspects of fluid-rock interactions in detachment zones. Geology 15, 362–366.

Rice, J.R., 1992. Fault stress states, pore pressure distributions, and the weakness of the San Andreas Fault. In: Evans, B., Wong, T.-F. (Eds.), Fault Mechanics and Transport Properties of Rocks. Academic press, New York, pp. 475–503.
Rooney, T., Furman, T., Yirgu, G., Ayalew, D., 2005. Structure of the Ethiopian lithosphere: xenolith evidence in the main Ethiopian rift. Geochim. Cosmochim. Acta 69, 3889–3910.
Rosendahl, B.R., 1987. Architecture of continental rifts with special reference to East Africa. Ann. Rev. Earth Planet. Sci. 15, 445–503.
Saria, E., Calais, E., Altamimi, Z., Willis, P., Farah, H., 2013. A new velocity field for Africa from combined GPS and DORIS space geodetic solutions: contribution to the definition of the African reference frame (AFREF). J. Geophys. Res. 118, 1–21.
Saria, E., Calais, E., Stamps, D.S., Delvaux, D., Hartnady, C.J.H., 2014. Present-day kinematics of the East African Rift. J. Geophys. Res. 119, 3584–3600.
Scholz, C.H., 2000. Evidence for strong San Andreas fault. Geology 28, 163–166.
Seno, T., Saito, A., 1994. Recent East African earthquakes in the lower crust. Earth Planet. Sci. Lett. 121, 125–136.
Sibson, R.H., 1974. Frictional constraints on thrust, wrench and normal faults. Nature 249, 542–544.
Sibson, R.H., 2000. Fluid involvement in normal faulting. J. Geodyn. 29, 469–499.
Sibson, R.H., Rowland, J.V., 2003. Stress, fluid pressure and structural permeability in seismogenic crust, North Island, New Zealand. Geophys. J. Int. 154, 584–594.
Stamps, D.S., Iaffaldano, G., Calais, E., 2015. Role of mantle flow in Nubia-Somalia plate divergence. Geophys. Res. Lett. 42. http://dx.doi.org/10.1002/2014GL062515.
Thatcher, W., Pollitz, F.F., 2008. Temporal evolution of continental lithospheric strength in actively deforming regions. GSA Today 18. http://dx.doi.org/10.1130/GSAT01804-5A.1.
Townend, J., Zoback, M.D., 2000. How faulting keeps the crust strong. Geology 28, 399–402.
Weinstein, A., Oliva, S.J., Ebinger, C.J., Roecker, S., Tiberi, C., Aman, M., Lambert, C., Witkin, E., Albaric, J., Gautier, S., Peyrat, S., Muirhead, J.D., Muzuka, A.N.N., Mulibo, G., Kianji, G., Ferdinand-Wambura, R., Msabi, M., Rodzianko, A., Hadfield, R., Illsley-Kemp, F., Fischer, T.P., 2017. Fault-magma interaction during early continental rifting: seismicity of the Magadi-Natron-Manyara basins, Africa. Geochem. Geophys. Geosyst. 18, 3662–3686. http://dx.doi.org/10.1002/2017GC007027.
Wessel, P., Smith, W., 1998. New, improved version of the generic mapping tools released. EOS Trans. AGU 79, 579.
Wilks, M., Ayele, A., Kendall, J-M., Wookey, J., 2016. The 24th January 2016 Hawassa Earthquake: implications for seismic hazard in the Main Ethiopian Rift. J. Afr. Earth Sci. 125, 118–125. http://dx.doi.org/10.1016/j.jafrearsci.2016.11.007.
Wolfenden, E., Ebinger, C., Yirgu, G., Deino, A., Ayalew, D., 2004. Evolution of the northern Main Ethiopian Rift: birth of a triple junction. Earth Planet. Sci. Lett. 224, 213–228.
Wright, T.J., Ebinger, C., Biggs, J., Ayele, A., Yirgu, G., Keir, D., Stork, A., 2006. Magma-maintained rift segmentation at continental rupture in the 2005 Afar diking episode. Nature 442, 291–294.
Zoback, M.L., 1992. Stress field constraints on intraplate seismicity in the Eastern North America. J. Geophys. Res. 97, 11,761–11,782.
Zoback, M.D., Townend, J., 2001. Implications of hydrostatic pore pressures and high crustal strength for the deformation of intraplate lithosphere. Tectonophysics 336, 19–30.
Zoback, M.D., Zoback, M.L., Mount, V.S., et al., 1987. New evidence on the state of stress of the San Andreas fault system. Science 238, 1105–1111.
Zoback, M.D., Zoback, M.L., 2002. Stress in the Earth's lithosphere. In: Third edition. Encyclopedia of Physical Science and Technology 16. pp. 143–154.